ORBIT CALCULATIONS ON THE EXTRACTION SYSTEM FOR THE MSU CYCLOTRON (*)

M.M. Gordon and H.G. Blosser
Michigan State University, East Lansing
(Presented by M.M. Gordon)

The calculations described here are relevant to the beam extraction system system which will be used when high external beam current with good energy resolution is desired. Extraction of H^- beams via electron-stripping will be used when a large duty factor is preferred to good energy resolution. The proposed extraction system is a modification of the "resonant-extraction" method[1] which incorporates advantageous features of the Berkeley system[2]. In the proposed scheme the ions are accelerated through the $\nu_r = 1$ resonance with a small field bump acting to drive the orbits off-center. As the value of ν_r drops sharply in the edge field, the displaced orbit centers undergo rapid precession thereby generating sufficient turn separation to facilitate entry into an electrostatic deflector. With a relatively short deflector, adequate clearance is achieved to permit use of a magnetic channel which then completes the beam deflection.

These calculations were made for a preliminary magnetic field which differs somewhat from the field finally adopted for our machine. Although the conclusions are generally valid, the final design will differ in detail from the results given here.

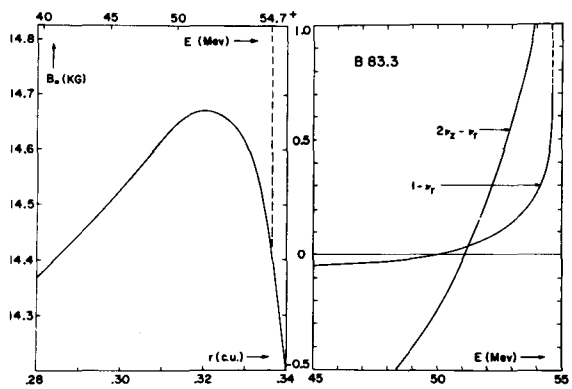

Fig. 1 Properties of "83.3" magnetic field : a) average magnetic field B_0 in kilogauss versus radius r in c.u. (1 c.u. = 90 in. for all results herein) and proton energy E in MeV; $\nu_r = 0$ at 54.7+ MeV. b) $(1 - \nu_r)$ and $(2\nu_z - \nu_r)$ versus E in edge region; $\nu_r = 1$ at $E^z = 50.1$ MeV, $2\nu_z = \nu_r$ at E = 51.1 MeV.

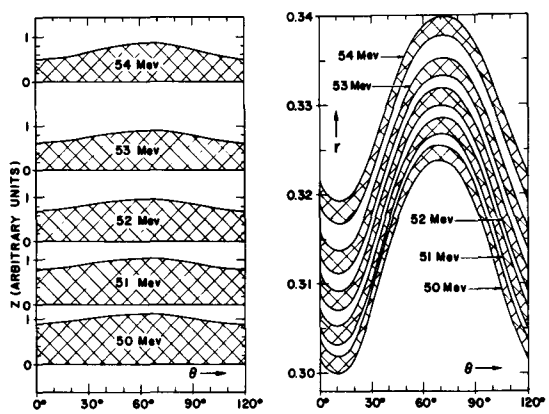

Fig. 2 Radial and axial profile of the beam from 50 to 54 MeV, obtained by assuming the (r,p_r) and (z,p_z) coordinates of the ions occupy eigenellipses of constant area. a) Radial width in c.u. of beam versus ϑ, normalized to $\Delta r = 0.2$ in. at $\vartheta = 0$, E = 50 MeV. b) Axial height |z| in arbitrary units versus ϑ. Note that the dees are positioned such that the dummy-dee region extends from $\vartheta = 45^0$ to $\vartheta = 90^0$ where the orbit protrusion is greatest, hence minimizing the area of the dees.

(*) Work supported by the National Science Foundation.

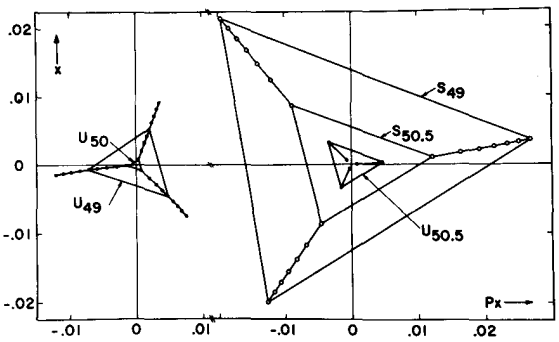

Fig. 3 Evolution of fixed-point diagram (ϑ = 45° to 50.5 MeV in 0.25 MeV steps; x = r - r_e in c.u. and $p_x = p_r - p_{re}$ in m_0c units, where (r_e, p_{re}) are the equilibrium orbit (EO) coordinates at the given energy. a) Contraction of the three unstable (U) fixed-points, which mark the stability limits, from 48 to 50 MeV. b) Contraction of stable fixed-points (open circles) from 49 to 50.5 MeV, and expansion of unstable fixed-points from 50.25 to 50.5 MeV. Note that beam occupies an approximately circular area of radius 0.001 c.u.

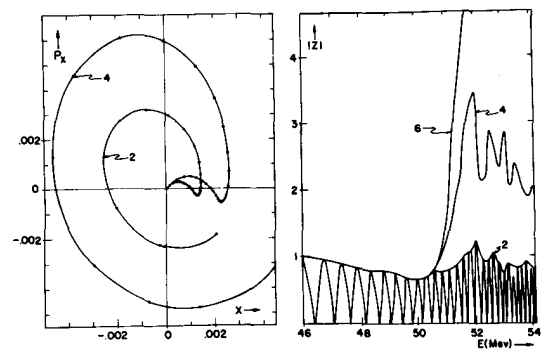

Fig. 5 Effects on accelerated orbits of field bumps : $b(r,\vartheta) = -h_1 \cos\vartheta$. a) Acceleration phase-plots showing x versus p_x, plotted once per turn at ϑ = 45°, for accelerated orbits starting on O E at E = 46 MeV, φ = -7.5°, for bump fields having h_1 = 2 and 4 gauss; plots show orbit-center displacement generated by field bump via ν_r = 1 resonance. b) Variation of axial oscillation amplitude |z| with energy E for these orbits (and also for orbit with H_1 = 6 gauss); plots show degree of axial instability produced by $\nu_r = 2\nu_z$ resonance (see Fig. 4)

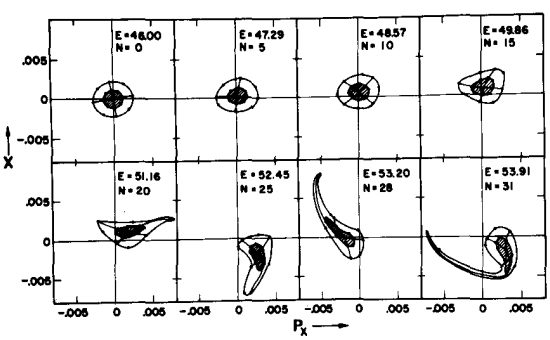

Fig. 7 Evolution of radial phase-space area associated with orbit "C" of Fig. 6b from 46 to 54 MeV. The inner "shaded" area which is bounded by the set of orbits "S", corresponds to the expected size of the beam.

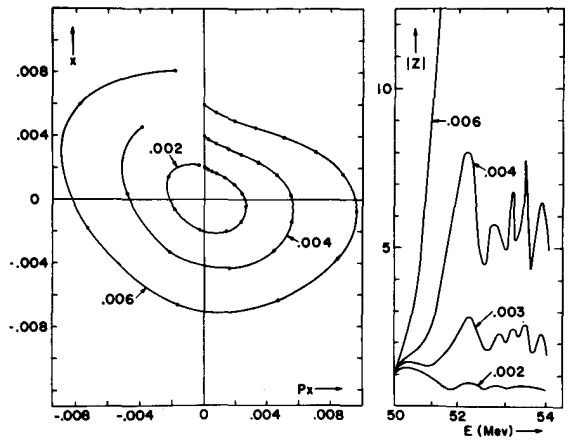

Fig. 4 Effect of radial oscillation amplitude on axial instability due to $\nu_r = 2\nu_z$ coupling resonance. a) Acceleration phase plots showing x versus p_x plotted once per turn at ϑ = 45° for three orbits accelerated from 50 to 54 MeV with initial x-displacements of 0.002, 0.004, and 0.006 c.u. b) Resultant variation of axial oscillation amplitude |z| with energy E for such orbits; |z| is normalized to unity at initial E = 50 MeV in each case. (The actual value of z in each case was taken sufficiently small to have negligible influence on the radial motion).

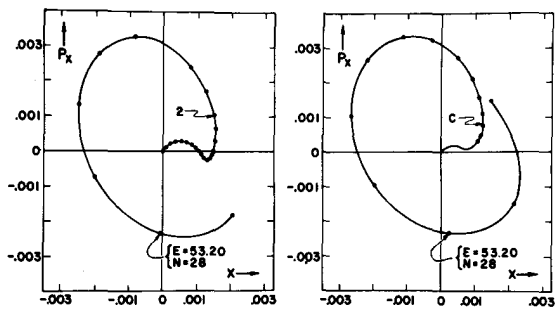

Fig. 6 Acceleration phase plots showing orbit-center displacement produced by two different bump fields. a) Orbit "2" for which h_1 = 2 gauss, independent of r (same as that shown in Fig. 5a). b) Orbit "C" with same initial conditions for which h_1 = 0 for r < 0.302 c.u., h_1 = 4 gauss for r > 0.325 c.u. and is nearly linear in between.

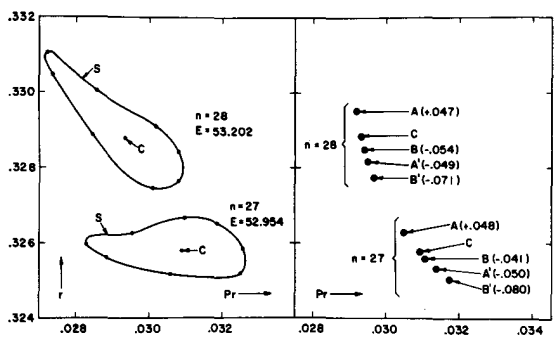

Fig. 8 (r,p_r) locations of orbits on turn n = 28 (ϑ = 45°) where electrostatic channel begins, and on previous turn n = 27 (ϑ = 45°). a) Orbit "C" (Fig. 6b) and orbit set "S" (shaded area of Fig. 7). b) Orbits A, A', B, B' relative to C; number in parenthesis gives energy difference relative to C in MeV.

The ions chosen for this study are protons which have about 53 MeV energy at extraction. Acceleration is accomplished by a two-dee system each dee having 70 kV to ground and an assumed angular width of 135°; thus, the peak energy gain/turn is $E_1 = (280)\cos(22.5^\circ) = 258$ keV/turn. Orbit computations were performed with the previously described General Oribt Code[3)]

Static Orbit Properties

The pertinent properties of static orbits in the extraction region of the field are displayed in Figs. 1-3. Since turn separation is to be achieved predominantly by displaced orbit center precession, extraction should commence above E = 52.5 MeV ($\nu_r < 0.9$). As shown in Fig. 2 maximum orbit separation occurs in the "valleys" at $\vartheta = 10^\circ$; the sector modulation of the oscillation amplitude produces a minimum radial beam width at $\vartheta \tilde{=} 58^\circ$; and the orientation of the dees requires that the electrostatic deflector begin at $\vartheta = 45^\circ$. The minimum in the axial beam width occuring at $\vartheta \tilde{=} 0^\circ$ may permit the insertion of probes to detect axial instability at the $\nu_r = 2\nu_z$ resonance. The fixed-point diagrams displayed in Fig. 3 demonstrate that the radial stability limits far exceed the phase-space area occupied by the beam, except from 49 MeV to 50.5 MeV; above 50.7 MeV "super-stability" obtains.

Limitations Imposed by Axial Stability

The maximum permissible orbit-center displacement which can be generated via the $\nu_r = 1$ resonance is set by the axial stability tolerance of the $\nu_r = 2\nu_z$ coupling resonance. Fig. 4 shows results for several orbits accelerated from 50 to 54 MeV with nearly constant radial amplitudes ranging from 0.002 to 0.006 c.u., and the resultant variation in z-amplitude for each. These results demonstrate that for radial amplitudes up to 0.002 c.u. the resonance has negligible effects; however, for sustained radial amplitudes > 0.003 c.u., the resonance has a disastrous effect on the axial motion.

Effects of Weak Field Bumps on Accelerated Orbits

The accelerated orbits in these extraction studies were started in the E.O. (equilibrium orbit) at E = 46 MeV with $\varphi = -7.5^\circ$ as "standard" initial conditions. At this energy the effect of the $\nu_r = 1$ resonance is negligible so that the assumption of initially centered orbits is realistic; $\varphi = -7.5^\circ$ was selected because it yields the best average energy gain/turn from 46 to 53 MeV. An initial study established that the radial amplitude induced by the electric gap-crossing resonance was inadequate for extraction purposes[4)]. The effects of various field bumps were therefore investigated. Fig. 5 shows results obtained with $b(r,\vartheta) = -h_1(r)\cos\vartheta$ field bumps having h_1 = 2, 4, and 6 gauss (independent of r); the amount of orbit-center displacement generated, via the $\nu_r = 1$ resonance, is nearly proportional to the bump strength (Fig. 5a); the corresponding axial motion is rather stable for the 2 gauss bump, but is quite unstable for bump strength $\geq$ 4 gauss (Fig. 5b).

Fig. 6 shows acceleration phase plots for two orbits: one (labeled "2") for

the 2 gauss bump field above; the other (labeled "C") for a field bump in which $h_1(r)$ is zero for r < 0.302 c.u., and rises to h_1 = 4 gauss for r > 0.325 c.u. At the energy chosen for extraction (53.2 MeV) the (x,p_x), and hence (r,p_r), values in both cases are nearly equal. This result indicates that the orbit-center displacement at extraction is determined mainly by the average bump strength near resonance, and is not sensitive to the detailed radial profile. A parallel study, varying the azimuthal location of the field bump, reveals that here again the (r,p_r) values at 53.2 MeV are relatively insensitive to such variations.

The field bump used in the studies described below is the one used for the orbit C of Fig. 6b; hence, this orbit forms the "central ray" for a family of orbits representing the beam behavior during extraction. The electrostatic channel begins at the point n = 28, E = 53.2 MeV marked in Fig. 6b; during the preceding turn, x increases by Δx = + 0.0021 c.u. = 0.19 in., and since the E.O. shifts by Δr_e = 0.08 in. At the same time, the net increase in r is Δr = 0.27 in.; hence, since the expected beam width is 0.20 in., this Δr should permit the beam to clear the septum at this point. A field with average strength of about 2 gauss poses problems of control; monitoring the axial amplitude at the $\nu_r = 2\nu_z$ resonance offers a possible solution to this problem.

Transmission of Radial and Axial Phase-Space through Resonances

A set of eight orbits were computed under conditions identical to that of the orbit C, but with initial (x,p_x) values on an eigen-ellipse representing the phase-space area of the beam (this set is hereafter designated "S"). A second set of eight such orbits were computed with (x,p_x) values twice that of S. The evolution of these radial phase-space areas is shown in Fig. 7; the "triangular" distortion produced by the ν_r = 3/3 resonance from n = 15 to n = 20 is apparent (compare with Fig. 3); the subsequent "shear" distortion due to the sharply falling edge-field is also apparent (n = 25 to n = 31). Since the latter distortion increases rapidly with energy, it is advisable to avoid accelerating the beam too far into the edge region of the field. For this reason 53.2 MeV was selected as the extraction energy. The results of Fig. 7 also clearly demonstrate the importance of having the ion orbits initially (46 MeV) well-centered.

Fig. 8a shows the $r\text{-}p_r$ configuration for the set of orbits S (and C) at $\vartheta = 45^\circ$ on turns n = 27 and n = 28; these areas have a radial separation Δr = 0.07 in. where the electrostatic channel septum would be inserted. Fig. 8b compares the $r\text{-}p_r$ locations of the orbit C with other orbits A-A' and B-B' whose initial conditions differ from C only in that: A-A' start at E = (46 ± .05) MeV; B-B' start with $\varphi = -7.5 \pm 7.5^\circ$. These results demonstrate that the resonance mechanism operating here is quite energy sensitive in that the (r,p_r) location of these orbits is correlated with their final energies. Variations in phase φ are significant mainly in that they translate into energy variations. Thus, the attainment of a highly efficient beam extraction system

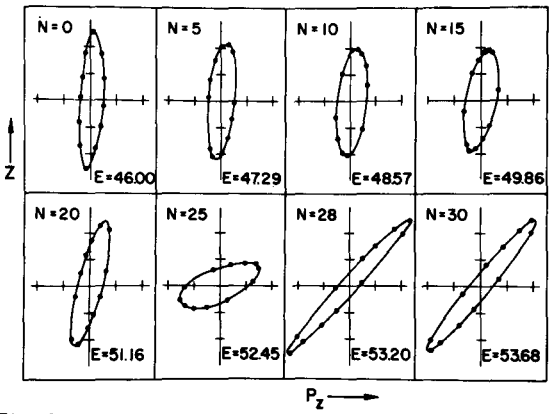

Fig. 9 Evolution of axial phase-space area associated with central ray orbit "C"; $\nu_r = 2\nu_z$ resonance occurs at E ≅ 51.1 MeV. (z scale is arbitrary).

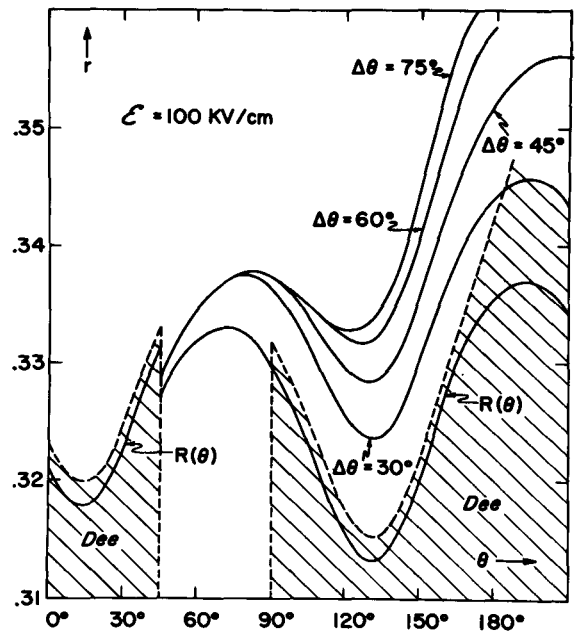

Fig. 10 r versus ϑ trajectories of orbit C and orbit set S traced through electrostatic channel and beyond; the electric field ϵ = 100 kV/cm acts only from ϑ = 45° to 105°. The cross-hatched area shows the Δr extent of the orbit set S for $\vartheta \geq 45°$.

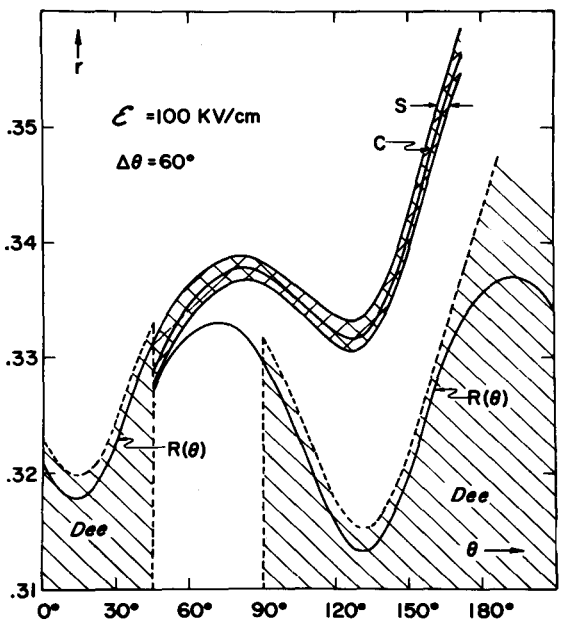

Fig. 11 r versus ϑ trajectory of orbit C for n = 28, $\vartheta \geq 45°$, showing effect of electrostatic deflector of different lengths. The electric field ϵ = 100 kV/cm acts transverse to the orbit from ϑ = 45° to 45° + Δθ; R(ϑ) is the maximum radial extent of the orbit set S (Fig. 7) for n ≦ 28, ϑ = 45°; the shaded portion indicates the area covered by the dees (dummy-dee extends from ϑ = 45° to 90°).

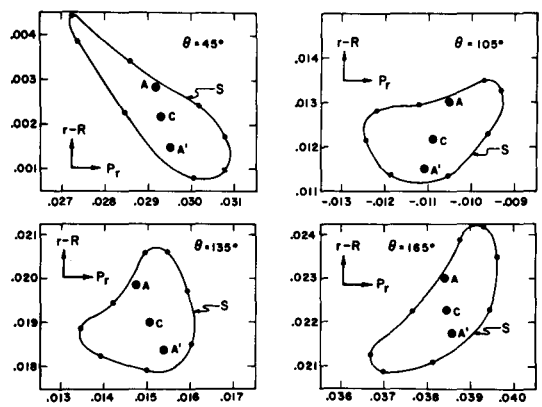

Fig. 12 Evolution of radial phase-space area from Fig. 8 (n = 28) traced through electrostatic channel (ϑ = 45° - 105°) and beyond (see Fig. 10). The (r - R) value gives the radial position relative to the maximum radial extent of the orbit set S on all previous turns.

requires a small energy spread within a given turn. To achieve an energy spread of only 100 keV within a single turn at 46 MeV requires a phase spread restriction $\Delta\varphi = 7.5^{\circ}$ at low energies; the possibility of achieving this goal is discussed elsewhere[5].

Fig. 9 shows the evolution of the axial phase-space area associated with the orbit C. Although the behavior of the z-motion is quite good under these conditions, it will not be as satisfactory for the entire orbit set S above, because of the sensitivity of axial stability to radial oscillation amplitude (see Fig. 4).

Effects of Electrostatic Deflector

The proposed electrostatic deflector has an electric field $\epsilon = 100$ kV/cm and a 1 cm aperture. Fig. 10 shows the effect on the orbit C of such a deflector beginning at n = 28, $\vartheta = 45^{\circ}$ (see Fig. 8a) and extending for different $\Delta\vartheta$ lengths. The curve $R(\vartheta)$ is the maximum extent of the orbit set S in Fig. 7 for $n \leqq 28$, $\vartheta = 45^{\circ}$. On the basis of these results a deflector length $\Delta\vartheta = 60^{\circ}$ was selected and subsequent computations assume this value.

The set of orbits S was tracked through the deflector and beyond; Fig. 11 shows the spread in r values for these orbits as a function of ϑ relative to the periphery of the dee and to $R(\vartheta)$. These results indicate at least 0.4 in. clearance between deflector and dee periphery for insulation space. The orbits are not sufficiently deflected by the electrostatic deflector and an additional magnetic channel is being planned. The latter will be introduced near $\vartheta = 130^{\circ}$, where the clearance between the orbits and dee periphery is about 1.4 in.

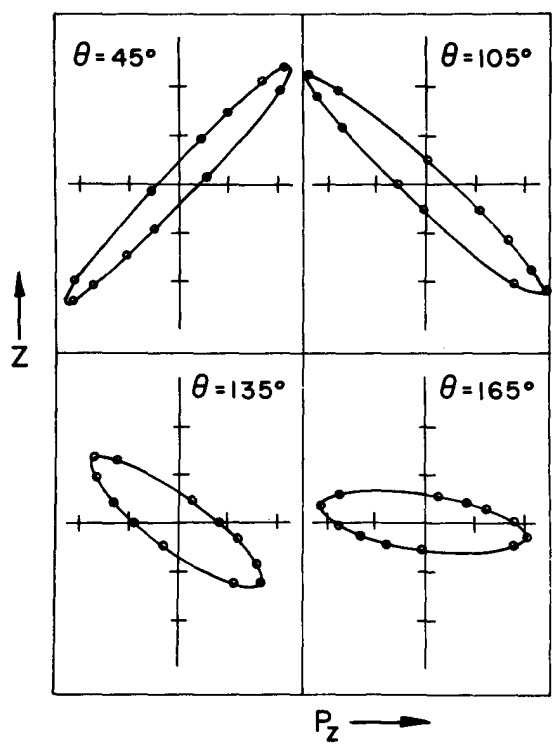

Fig. 13 Evolution of axial phase-space area from Fig. 9 (n = 28) traced through electrostatic channel ($\vartheta = 45^{\circ} - 105^{\circ}$) and beyond; corresponding radial motion is that of orbit C in Fig. 11.

Fig. 12 shows (r-R) versus p_r plots at several ϑ values for the orbit set S from Fig. 11, and also for the orbits A-A' of Fig. 8b. As can be seen, the radial phase-space area maintains its good focusing character into the edge region of the field; also apparent is the transmission of the orbits A-A' with ± 50 keV energy difference from C. Fig. 13 shows the corresponding axial phase-space behavior obtained by continuing the orbits of Fig. 9 through the channel and beyond; the sharp increase in axial focusing in this region is evident.

References

1. Blosser, Gordon, and Arnette, Nuc. Instr. and Meth., 18-19, 488 (1962).
2. Garren, Judd, Smith and Willax, ibid., 525.
3. Arnette, Blosser, Gordon and Johnson, ibid., 343.
4. M.M. Gordon, ibid., 268.
5. Blosser, Gordon, and Reiser, see paper V-4.

DISCUSSION

LAPOSTOLLE : What extraction efficiency do you expect with this system?

GORDON : It depends on several factors, you could presumably get very good deflection efficiency, let us say over 80 percent.

MARTIN : You previously studied systems using a much stronger bump, invoking the non-linear resonance, would you care to comment on your reasons for your change?

GORDON : Yes, those systems involving the non-linear resonant extraction are well adapted for a machine accelerating a single ion to a fixed energy. We are moving toward a machine which will accelerate many different ions to many different final energies and, therefore, must have the greatest possible flexibility. Accelerating the beam far into the edge region of the field, within certain constraints, is the best way to achieve this flexibility.

BLOSSER : On the matter of efficiency, if you can control the field bump you can get 100% efficiency for particles leaving the source at a given instant; the overall efficiency then depends only on how well you succeed in trimming the interval of RF phases that leave the source.

GORDON : This is a question of where you define the beam, on the septum and in the channel or, alternatively, near the source to avoid the loss later.

WALKINSHAW : What field strength do you require for extraction?

GORDON : For the calculations we assumed 100 kV/cm with an aperture of about 1 cm. Considering the information we received here at the conference it appears that we could get 150 kV/cm on a 1 cm aperture. In that case we can deflect the beam without the additional magnetic channel.